Acta Crystallographica Section D
Biological Crystallography
ISSN 1399-0047

Crystal structures and catalytic mechanism of the *C*-methyltransferase Coq5 provide insights into a key step of the yeast coenzyme Q synthesis pathway

Ya-Nan Dai,‡ Kang Zhou,‡ Dong-Dong Cao, Yong-Liang Jiang, Fei Meng, Chang-Biao Chi, Yan-Min Ren, Yuxing Chen and Cong-Zhao Zhou*

Hefei National Laboratory for Physical Sciences at the Microscale and School of Life Sciences, University of Science and Technology of China, Hefei, Anhui 230027, People's Republic of China

‡ These authors contributed equally to this work.

Correspondence e-mail: zcz@ustc.edu.cn

Received 23 January 2014
Accepted 19 May 2014

PDB references: Coq5, apo, 4obx; SAM-bound, 4obw

Saccharomyces cerevisiae Coq5 is an *S*-adenosyl methionine (SAM)-dependent methyltransferase (SAM-MTase) that catalyzes the only *C*-methylation step in the coenzyme Q (CoQ) biosynthesis pathway, in which 2-methoxy-6-polyprenyl-1,4-benzoquinone ($DDMQH_2$) is converted to 2-methoxy-5-methyl-6-polyprenyl-1,4-benzoquinone ($DMQH_2$). Crystal structures of Coq5 were determined in the apo form (Coq5-apo) at 2.2 Å resolution and in the SAM-bound form (Coq5-SAM) at 2.4 Å resolution, representing the first pair of structures for the yeast CoQ biosynthetic enzymes. Coq5 displays a typical class I SAM-MTase structure with two minor variations beyond the core domain, both of which are considered to participate in dimerization and/or substrate recognition. Slight conformational changes at the active-site pocket were observed upon binding of SAM. Structure-based computational simulation using an analogue of $DDMQH_2$ enabled us to identify the binding pocket and entrance tunnel of the substrate. Multiple-sequence alignment showed that the residues contributing to the dimeric interface and the SAM- and $DDMQH_2$-binding sites are highly conserved in Coq5 and homologues from diverse species. A putative catalytic mechanism of Coq5 was proposed in which Arg201 acts as a general base to initiate catalysis with the help of a water molecule.

1. Introduction

Coenzyme Q (ubiquinone or CoQ) is a lipid-soluble compound that serves as one of the most important electron carriers of the respiratory chain in both prokaryotes and eukaryotes (Hsieh *et al.*, 2007). CoQ comprises a fully substituted benzoquinone ring connected to a long hydrophobic polyprenyl side chain. The benzoquinone ring is responsible for the redox activity, whereas the polyprenyl tail mediates membrane anchoring (Tauche *et al.*, 2008). The number of isoprene units varies among different species from six in *Saccharomyces cerevisiae* (CoQ_6) to ten in humans (CoQ_{10}). In addition, the reduced ubiquinol form of CoQ is a recyclable lipophilic antioxidant that protects membrane phospholipid layers, mitochondrial DNA and membrane proteins against oxidative damage (Johnstone *et al.*, 2007; Brindley *et al.*, 2003; Lee *et al.*, 2012). Deficiency of CoQ_{10} in humans has been reported to be associated with many major clinical phenotypes (Binz *et al.*, 2010). Therefore, CoQ_{10} is an essential micronutrient in humans owing to its antioxidant function.

Generally, demand for CoQ in cells relies on its *de novo* synthesis. The CoQ biosynthesis pathway in eukaryotes is mostly based on findings in yeast (Tran & Clarke, 2007). To date, nine genes designated *COQ1–COQ9* have been

identified to be involved in CoQ_6 biosynthesis. Biosynthesis usually starts with formation of the aromatic precursor *para*-hydroxy-
benzoic acid or *para*-aminobenzoic acid and the polyprenyl chain (Hsieh *et al.*, 2007; Pierrel *et al.*, 2010; Braun *et al.*, 2010). Afterwards, modifications of the aromatic ring including *O*-methylation, decarboxylation and *C*-methylation take place in order to generate mature CoQ_6. It has been suggested that a large complex comprising the Coq enzymes (Coq1–Coq9) is peripherally associated with the mitochondrial inner membrane to catalyze these successive reactions (Tran & Clarke, 2007). To date, no structure of any enzyme from the CoQ_6 biosynthesis pathway has been reported.

Coq5 has been shown to be a core component of this complex since it is required for the stability and activity of several components based on biochemical studies (Baba *et al.*, 2004). Coq5 is an *S*-adenosyl methionine (SAM)-dependent methyltransferase (SAM-MTase) that catalyzes the only *C*-methylation step, which converts 2-methoxy-6-polyprenyl-1,4-benzoquinone ($DDMQH_2$) to 2-methoxy-5-methyl-6-polyprenyl-1,4-benzoquinone ($DMQH_2$) in the CoQ_6 biosynthesis pathway (Fig. 1).

Various C_1-transfer reactions towards small molecules or macromolecules during metabolism, cell signalling and epigenetic programming are catalyzed by MTases using SAM as the methyl donor (Grove *et al.*, 2011). Currently, SAM-MTases are categorized into five classes (I–V) according to their structural features (Schubert *et al.*, 2003). Class I represents the largest group of MTases possessing a Rossmann-like fold and contains a very large variety of MTases transferring methyl groups from SAM to either O, N or C atoms, which are thus called O-MTases, N-MTases and C-MTases, respectively. To our current knowledge, the mechanisms of O-MTases and N-MTases have been studied extensively (Woodard, Mascaro *et al.*, 1980; Lee *et al.*, 2010; Takata *et al.*, 2003; Carney & Holden, 2011; Lee *et al.*, 2012), in which an S_N2-type mechanism is employed to methylate their substrates with a nucleophilic attack on the methyl group of SAM and the release of *S*-adenosyl homocysteine (Hegazi *et al.*, 1979, Woodard, Tsai *et al.*, 1980). In particular, the active sites of O-MTases and N-MTases usually comprise a conserved histidine residue and/or a tyrosine residue (Takata *et al.*, 2003, Carney & Holden, 2011; Lee *et al.*, 2010, 2012). In contrast, the catalytic mechanisms of C-MTases seem to be more complicated and have been much less well elucidated. It has been proposed that C-MTases also employ an S_N2-type mechanism, except for DNA (cytosine-C5)-MTases, which use a conserved cysteine to enhance the reactivity of the target C atom (Wu & Santi, 1987). However, the fine catalytic mechanism of C-MTases towards the nucleophilic C atoms of diverse secondary metabolites such as enolizable ketones (Mahlert *et al.*, 2007; Braun *et al.*, 2010; Chen *et al.*, 2001) and phenolic substrates (including $DDMQH_2$; Fawaz & Jones, 1988; Lee *et al.*, 1997; Crnovčić *et al.*, 2010) remains largely unknown.

Here, we report the crystal structures of yeast Coq5 in the apo form (Coq5-apo) and SAM-bound form (Coq5-SAM) at 2.2 and 2.4 Å resolution, respectively. The overall structure of Coq5 displays a dimer, each subunit of which has a core domain with the typical topology of the class I SAM-MTases. Beyond the core domain, there are two minor variations which are both responsible for the dimeric interaction and/or the $DDMQH_2$ substrate specificity. As a consequence of SAM binding, the side chains of both Asn179 and Asn202 are pulled towards the active-site pocket. Furthermore, we determined a putative substrate-entrance tunnel by structure-based computational simulation using a $DDMQH_2$ substrate analogue. Multiple sequence alignment showed that the residues contributing to the dimeric interface and the substrate-binding pocket are highly conserved in Coq5 and homologues from diverse species. Taking these results together, we proposed a putative catalytic mechanism for Coq5.

2. Materials and methods

2.1. Cloning, overexpression and purification of Coq5-ΔN26

A truncated sequence of the *COQ5*/*YML110C* gene without the signal peptide (Met1–Ala26, termed Coq5-ΔN26) was amplified from the genomic DNA of *S. cerevisiae* S288c and cloned into a pET-28a-derived expression vector with an N-terminal 6×His tag. The recombinant plasmid was transformed into *Escherichia coli* BL21 (DE3) strain (Novagen) cultured in LB culture medium (10 g NaCl, 10 g Bacto tryptone and 5 g yeast extract per litre) containing 30 μg ml^{-1} kanamycin at 37°C. When the cells had grown to an $OD_{600\ nm}$ of 0.8, expression of the protein was induced with 0.2 m*M* isopropyl β-D-1-thiogalactopyranoside and cell growth continued for a further 20 h at 16°C before harvesting. Cells were collected and resuspended in lysis buffer [100 m*M* NaCl, 5%(*v*/*v*) glycerol, 20 m*M* Tris–HCl pH 8.0]. After 30 min of sonication and centrifugation at 12 000*g* for 30 min, the supernatant containing the soluble target protein was collected and loaded onto a nickel-chelating column (GE Healthcare) equilibrated with binding buffer

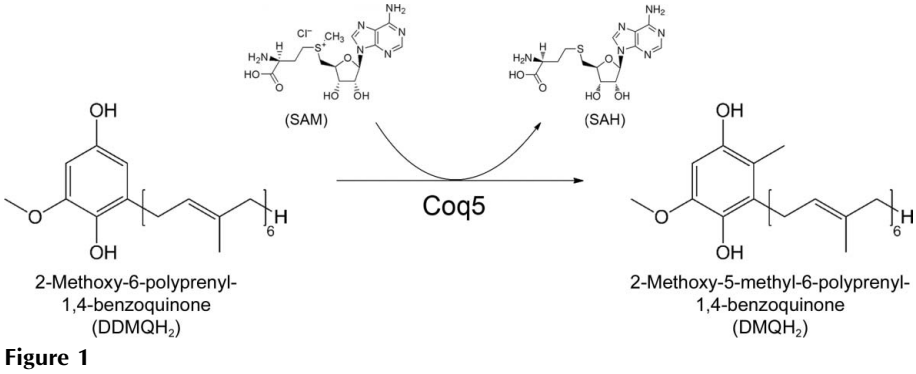

Figure 1
Conversion of 2-methoxy-6-polyprenyl-1,4-benzoquinone ($DDMQH_2$) to 2-methoxy-5-methyl-6-polyprenyl-1,4-benzoquinone ($DMQH_2$) by yeast Coq5.

Table 1
Crystal parameters, data collection and structure refinement.

Values in parentheses are for the highest resolution bin.

	Se-Coq5	Coq5-apo	Coq5-SAM
Data collection			
Space group	$P6_222$	$C2$	$C2$
Unit-cell parameters			
a (Å)	108.92	193.27	193.34
b (Å)	108.92	75.64	74.96
c (Å)	102.20	84.48	84.08
α (°)	90.00	90.00	90.00
β (°)	90.00	90.85	91.85
γ (°)	120.00	90.00	90.00
Resolution range (Å)	50.00–3.00 (3.16–3.00)	49.04–2.20 (2.32–2.20)	42.69–2.40 (2.53–2.40)
Wilson B factor (Å^2)	75.66	32.23	33.06
Unique reflections	7618 (1072)	61136 (8943)	43628 (6301)
Completeness (%)	100.0 (100.0)	98.7 (99.3)	92.7 (92.5)
Anomalous multiplicity	20.5 (20.3)		
Anomalous completeness (%)	100.0 (100.0)		
$R_{\rm merge}$†	0.156 (1.042)	0.074 (0.511)	0.084 (0.286)
Average multiplicity	36.6 (37.7)	3.9 (3.7)	3.7 (3.3)
Phasing statistics			
Correlation coefficient	0.51		
Figure of merit	0.232		
Structure refinement			
Resolution range (Å)		50.00–2.20	42.69–2.40
R factor‡/$R_{\rm free}$§		0.207/0.248	0.236/0.283
No. of protein atoms		7500	7470
No. of water atoms		435	363
R.m.s.d.¶, bond lengths (Å)		0.006	0.005
R.m.s.d.¶, bond angles (°)		1.068	0.904
Mean B factor (Å^2)		34.84	34.37
Ramachandran plot††			
Poor rotamers (%)		0.86	0.62
Most favoured (%)		97.96	97.41
Additional allowed (%)		2.04	2.59
Outliers (%)		0	0
Clashscore (per 1000 atoms)		4.64	1.80
PDB entry		4obx	4obw

† $R_{\rm merge} = \sum_{hkl}\sum_i |I_i(hkl) - \langle I(hkl)\rangle| / \sum_{hkl}\sum_i I_i(hkl)$, where $I_i(hkl)$ is the intensity of an observation and $\langle I(hkl)\rangle$ is the mean value for its unique reflection; summations are over all reflections. ‡ R factor $= \sum_{hkl} ||F_{\rm obs}| - |F_{\rm calc}|| / \sum_{hkl} |F_{\rm obs}|$, where $F_{\rm obs}$ and $F_{\rm calc}$ are the observed and calculated structure-factor amplitudes, respectively. § $R_{\rm free}$ was calculated with 5% of the data excluded from the refinement. ¶ Root-mean-square deviation from ideal values (Engh & Huber, 1991). †† Categories were defined by *MolProbity*.

[100 m*M* NaCl, 5%(*v*/*v*) glycerol, 20 m*M* Tris–HCl pH 8.0]. The target protein was eluted with 300 m*M* imidazole and loaded onto a HiLoad 16/60 Superdex 200 column (GE Healthcare) pre-equilibrated with 100 m*M* NaCl, 5%(*v*/*v*) glycerol, 20 m*M* Tris–HCl pH 8.0. Fractions containing the target protein were pooled and were concentrated to 5 mg ml^{-1} for crystallization. Protein purity was then assessed by SDS–PAGE.

2.2. Mapping of the core domain of Coq5

Coq5-ΔN26 was first screened for crystallization, but no crystals were obtained. Therefore, we performed partial digestion of Coq5-ΔN26 using the protease trypsin combined with liquid-chromatography mass spectrometry to define a compact domain covering 247 residues corresponding to Ser61–Val307, indicating that the segment at the N-terminus comprising residues His27–Lys60 is relatively flexible. The truncated sequence (residues Ser61–Vla307, designated Coq5) was then subcloned, overexpressed and purified in the same way as described above for Coq5-ΔN26.

2.3. Incorporation of selenomethionine into Coq5

Selenomethionine (SeMet)-labelled Coq5 (Se-Coq5) protein was overexpressed in *E. coli* strain B834 (DE3) (Novagen). A culture of transformed cells was inoculated into LB medium and incubated at 37°C. The cells were harvested when the $OD_{600\ nm}$ reached 0.2 and were washed twice with M9 medium. The cells were then cultured in SeMet medium (M9 medium with 25 mg l^{-1} SeMet and the other essential amino acids at 50 mg l^{-1}) to an $OD_{600\ nm}$ of 0.6–0.8. The remaining steps of protein expression, purification and storage of Se-Coq5 were the same as for native Coq5.

2.4. Crystallization, data collection and processing

Screening for crystallization conditions of Coq5-apo and Coq5-SAM was performed using Crystal Screen, Crystal Screen 2, Index, Grid Screen and SaltRx (Hampton Research) by the hanging-drop vapour-diffusion method in 96-well plates at 16°C. During optimization in 24-well plates, native crystals of Coq5-apo were grown by mixing 3 µl 5 mg ml^{-1} protein sample (with 5 m*M* DTT added) with 1 µl reservoir solution [20%(*w*/*v*) 2-propanol, 20%(*w*/*v*) polyethylene glycol 4000, 0.1 *M* sodium citrate tribasic pH 5.6] and equilibrating against 0.1 ml reservoir solution. Native crystals of Coq5–SAM were obtained by co-crystallization with 5 m*M* SAM using the same technique with a reservoir consisting of 20%(*w*/*v*) polyethylene glycol 3350, 0.2 *M* ammonium citrate tribasic pH 7.0. Additionally, crystals of Se-Coq5 were obtained using the same method with a reservoir consisting of 0.2 *M* sodium citrate tribasic, 30%(*w*/*v*) polyethylene glycol 400, 0.1 *M* Tris–HCl pH 8.5. Typically, crystals appeared in 1–2 d and reached maximum size in one week. The crystals were transferred to cryoprotectant (reservoir solution supplemented with 25% glycerol) and flash-cooled in liquid nitrogen. Both native and SeMet-derivative data sets were collected from single crystals at 100 K in a liquid-nitrogen stream on beamline 17U using an ADSC Q315r CCD detector at the Shanghai Synchrotron Radiation Facility (SSRF). All diffraction data were indexed, integrated and scaled with *iMosflm* (Battye *et al.*, 2011).

2.5. Structure determination and refinement

The crystal structure of Coq5 was determined by the single-wavelength anomalous dispersion phasing method using data from a single SeMet-substituted protein crystal to a maximum resolution of 3.0 Å. The *AutoSol* program from *PHENIX* (Adams *et al.*, 2010) was used to locate the heavy atoms, and the phases were calculated and further improved using partial model extension in *OASIS* (Hao *et al.*, 2000). Automatic model building was carried out using *AutoBuild* in *PHENIX*. The initial model was then used for molecular replacement with the native data set of Coq5-SAM at 2.4 Å resolution with *MOLREP* (Vagin & Teplyakov, 2010). Refinement was carried out using the maximum-likelihood method implemented in *REFMAC*5 (Murshudov *et al.*, 2011) as part of the *CCP*4 suite

(Winn *et al.*, 2011) and the model was rebuilt interactively using *Coot* (Emsley & Cowtan, 2004). The final model was evaluated with *MolProbity* (Chen *et al.*, 2010) and *PROCHECK* (Laskowski *et al.*, 1993). In addition, the structure of Coq5-apo was determined by *MOLREP* using the coordinates of Coq5-SAM as the search model. Refinement and evaluation were performed using the same programs as used for Coq5-SAM. Crystallographic parameters and data-collection statistics are listed in Table 1. All structure figures were prepared with *PyMOL* (Schrödinger).

2.6. Remodelling of the substrate-binding site

To elucidate the structural basis for the binding of the $DDMQH_2$ substrate, we attempted to determine the structure of Coq5 in complex with several types of $DDMQH_2$ analogues

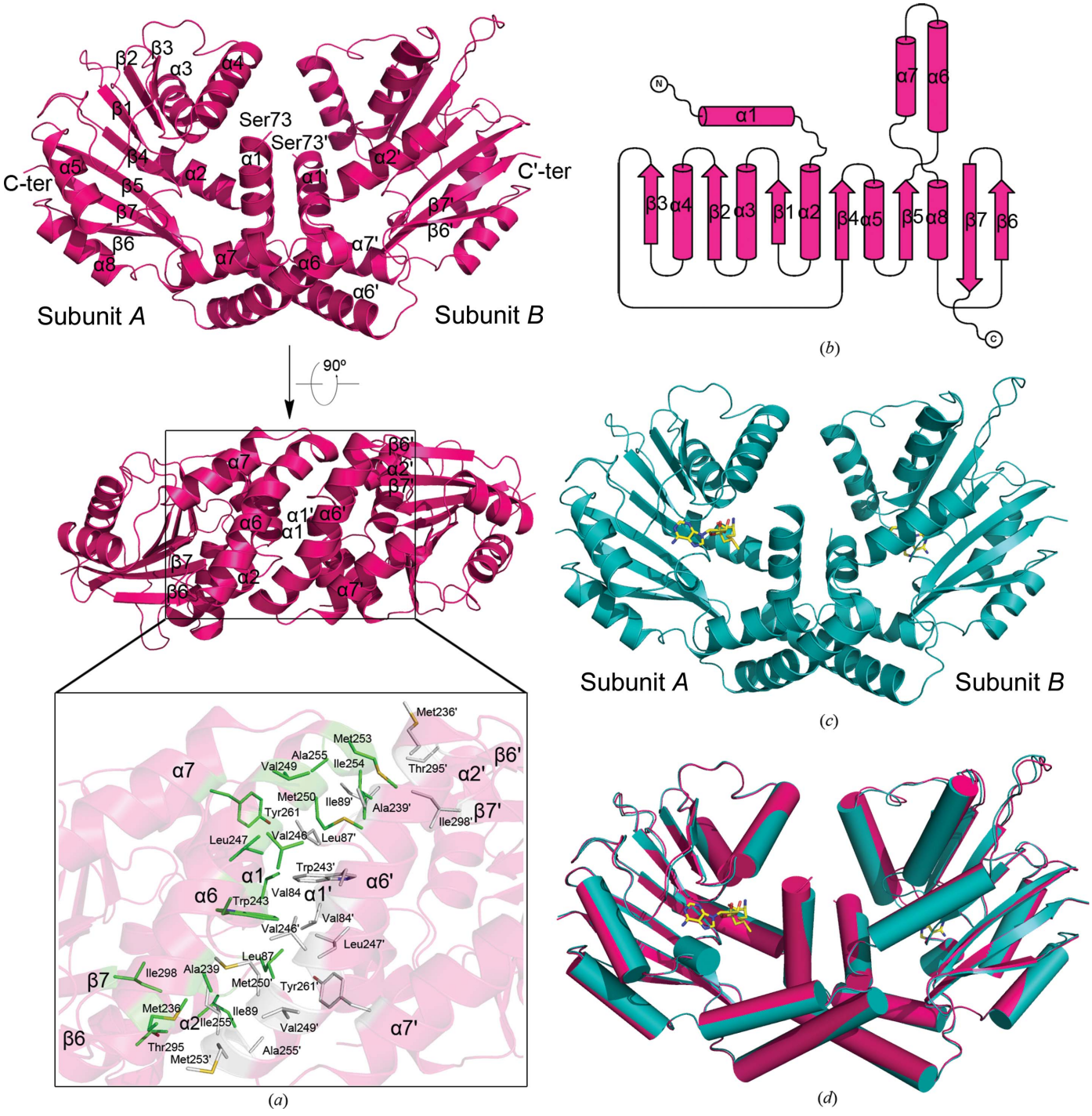

Figure 2
Overall structure of yeast Coq5. (*a*) The Coq5-apo dimer is coloured red. Residues involved in the dimeric interaction are shown as green (subunit *A*) and grey (subunit *B*) sticks, respectively. (*b*) Topology diagram of Coq5-apo. (*c*) The Coq5-SAM dimer is coloured cyan, with SAM shown as yellow sticks. (*d*) Superposition of the overall structures of Coq5-apo and Coq5-SAM.

owing to the lack of commercial availability of the natural substrate $DDMQH_2$. However, both co-crystallization and soaking methods failed. Alternatively, we simulated a model of the ternary complex of Coq5-SAM with a $DDMQH_2$ analogue (with two isoprene units) using *AutoDock* (Morris *et al.*, 2009). The three-dimensional structure of the $DDMQH_2$ analogue was transformed with the *PRODRG* server (Schüttelkopf & van Aalten, 2004). After the modelling process, up to ten poses were generated in three output clusters, among which a cluster containing seven members was in the lowest energy state.

3. Results and discussion

3.1. Overall structures of Coq5-apo and Coq5-SAM

To elucidate the structural basis of the catalytic mechanism, we solved the structures of Coq5-apo and Coq5-SAM at 2.2 and 2.4 Å resolution, respectively. We used the truncated version of Coq5-ΔN60 spanning residues Ser61–Vla307 for crystallization; however, residues Ser61–Ser72 could not be traced in the electron-density maps, indicating high flexibility of this N-terminal segment. Both crystals belonged to space group *C*2, with two dimers in the asymmetric unit. The dimeric interfaces of the two structures bury total surface areas of 1039 and 1066 Å^2, respectively, implying that the structures are folded into dimeric forms with two tightly associated subunits (Figs. 2*a* and 2*c*). Gel-filtration chromatography also indicated that Coq5 exists as a dimer in solution (data not shown). In addition, the Coq5 structures were predicted to be dimers by interface analysis using *PDBePISA* (Krissinel & Henrick, 2007).

The overall structure of Coq5-apo exhibits a typical SAM-MTase topology incorporating a mixed α/β topology as the core domain (Fig. 2*b*). This domain represents a Rossmann-like fold composed of six parallel β-strands (β1–β6) surrounded by five α-helices (α2–α5 and α8) at each side with strand β7 antiparallel to the other strands. There are two minor variations beyond the core domain of Coq5, both of which are considered to be relatively common features of all small-molecule SAM-MTases (Martin & McMillan, 2002). The first is the addition of an N-terminal helix α1, which has been

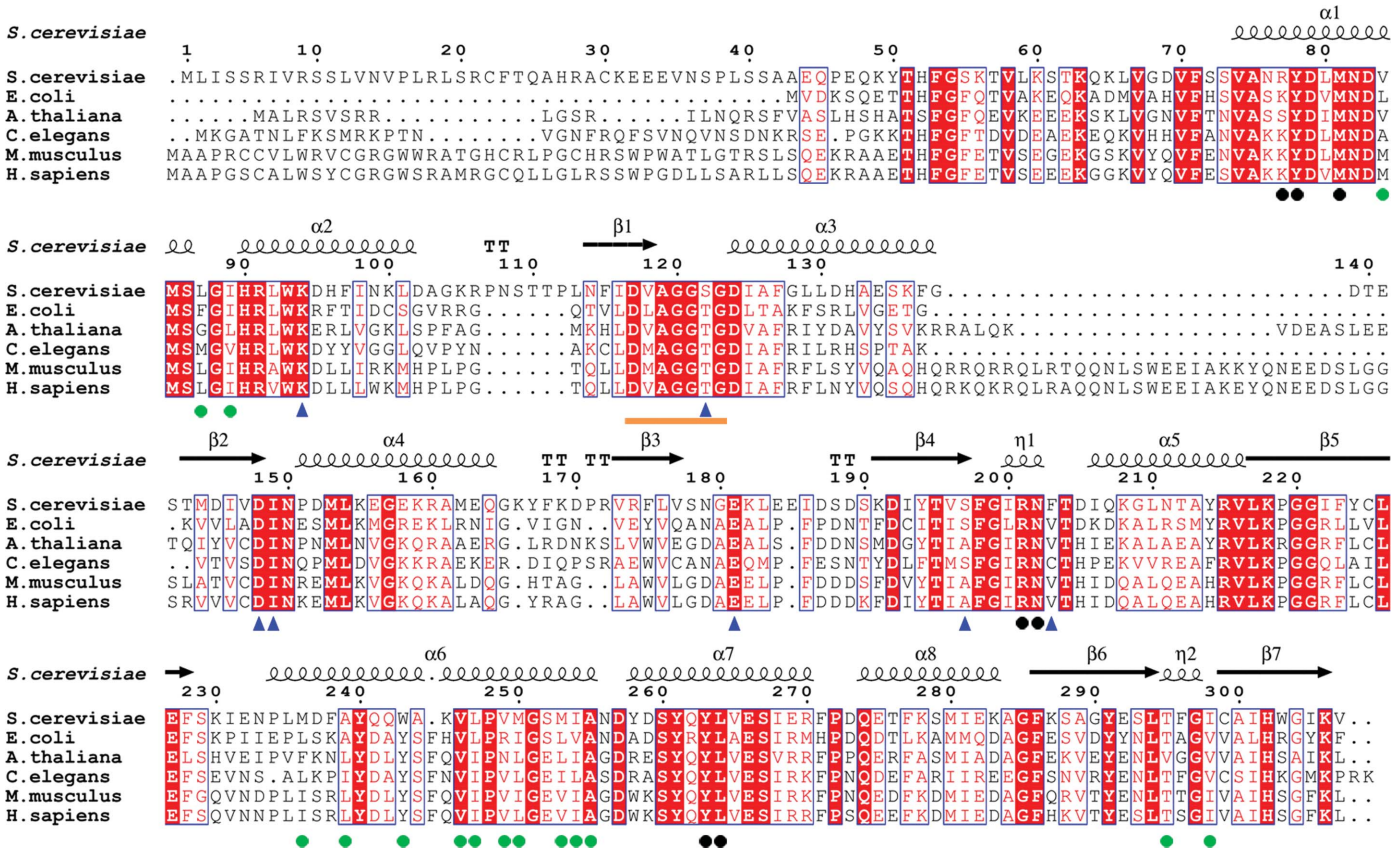

Figure 3
Multiple sequence alignment of Coq5 and homologues. The DVAGGSG segment is indicated by an orange line and other residues involved in binding SAM are indicated with blue triangles. The residues contributing to interface formation are indicated with green dots. The residues responsible for the formation of the $DDMQH_2$ substrate analogue-binding cavity are indicated with black dots. The multiple sequence alignment was performed using *ClustalW*2 (http://www.ebi.ac.uk/Tools/msa/clustalw2/) and *ESPript* (http://espript.ibcp.fr/ESPript/cgi-bin/ESPript.cgi). All sequences were downloaded from the NCBI database (http://www.ncbi.nlm.nih.gov). The sequences are (NCBI accession Nos. are given in parentheses) *S. cerevisiae* S288c 2-hexaprenyl-6-methoxy-1,4-benzoquinone methyltransferase Coq5 (NP_013597.1), *Escherichia coli* EDL933 ubiquinone/menaquinone biosynthesis methyltransferase (NP_290465.1), *Arabidopsis thaliana* 2-methoxy-6-polyprenyl-1,4-benzoquinol methylase (NP_200540.1), *Caenorhabditis elegans* Bristol N2 protein Coq5 (NP_498704.1), *Mus musculus* C57BL/6 2-methoxy-6-polyprenyl-1,4-benzoquinol methylase (NP_080780.1) and *Homo sapiens* 2-methoxy-6-polyprenyl-1,4-benzoquinol methylase (NP_115690.3).

reported to usually function as a 'lid' to cover the active site of small-molecule SAM-MTases (Vidgren *et al.*, 1994; Fu *et al.*, 1996). The second is an insertion of two helices (α6 and α7) between β5 and α8. Both variations participate in the dimeric interaction, with the major contribution being from α6. In addition, helices α1 and α7 also contribute part of the active-site pocket.

The dimeric interface is mainly stabilized by hydrophobic interactions between 32 residues from both subunits (Fig. 2*a*). The largest interface area is made up of ten residues from α6: Met236, Ala239, Trp243, Val246, Leu247, Val249, Met250, Met253, Ile254 and Ala255. In addition, six residues (Val84 from α1, Leu87 and Ile89 from the loop connecting α1 and α2, Tyr261 from α7 and Thr295 and Ile298 from the loop connecting β6 and β7) also take part in the dimeric interaction. Multiple sequence alignment showed that these residues are highly conserved in Coq5 and homologues from diverse species (Fig. 3).

In the Coq5-SAM structure, a molecule of SAM is deeply buried in the active-site cleft (Fig. 2*c*). Superposition of Coq5-SAM on Coq5-apo yields an overall root-mean-square deviation of 0.35 Å over 423 C^{α} atoms of the dimers (Fig. 2*d*). It is notable that the dimeric interface is slightly increased from 1039 to 1066 Å^2 upon binding SAM, further indicating that dimerization is necessary for the activity of Coq5.

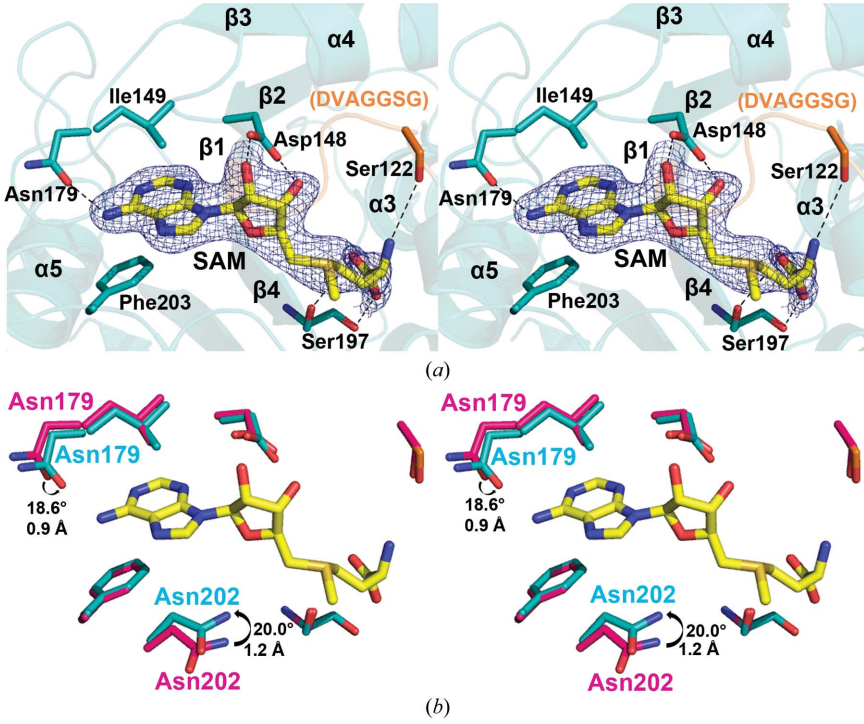

Figure 4
Stereoview of the SAM-binding site. (*a*) SAM (yellow) is shown as thick sticks. The SAM molecule is superimposed with the $2F_o - F_c$ electron-density map contoured at 1σ (0.2331 e Å^{-3}). Residues involved in SAM interaction are shown as sticks. Polar interactions are indicated by dashed lines. The glycine-rich sequence DVAGGSG is coloured orange. (*b*) Superposition of the SAM-binding region. Residues are shown as sticks in red (apo form) and cyan (SAM complex), respectively. Conformational changes are indicated by black arrows.

3.2. The SAM-binding site

Electron density for SAM is clearly defined within each subunit of the complex structure. Taking monomer *A* as an example, the SAM molecule is mainly fixed by a network of hydrogen bonds and hydrophobic interactions that is largely conserved among small-molecule SAM-MTases (Fig. 4*a*). Residues involved in SAM interaction are located on four loops which connect β1 to α3, β2 to α4, β3 to β4 and β4 to α5. The adenine ring is stabilized by a hydrogen bond to the side chain of Asn179, in addition to hydrophobic interaction with the side chain of Ile149 and π–π stacking against the benzene ring of Phe203. The ribose group is fixed by two hydrogen bonds to the side chain of Asp148. Moreover, the carboxyl and amino groups of the methionine moiety of SAM are involved in hydrogen bonding to Ser122 and Ser197. Notably, residues Lys94 and Asp124 also participate in stabilizing the methionine moiety of SAM in other monomers of Coq5 (Supplementary Fig. S2[1]). In addition, the universal glycine-rich motif E/D*X*G*X*G*X*G in SAM-MTases is found as DVAGGSG in Coq5, with a minor variation of Ala119 instead of a glycine. Multiple-sequence alignment showed that these residues are highly conserved in Coq5 from diverse species (Fig. 3). Upon binding SAM, the side chains of Asn179 and Asn202 are pulled towards the centre of the active-site pocket by 18.6° and 20.0° (Fig. 4*b*). As a consequence, Asn179 is able to interact with the adenine ring of SAM, whereas Asn202 is more likely to be involved in stabilizing the approaching substrate $DDMQH_2$.

3.3. The active site and putative substrate-binding pattern

In the simulated model, the $DDMQH_2$ analogue fits well into a cavity adjacent to the leaving methyl group of SAM (Fig. 5*a*). In addition to hydrophobic interactions with the four residues Tyr78, Met81, Tyr263 and Leu264, the analogue is further fixed by two hydrogen bonds to the side chains of Arg77 and Asn202. More important, superimposing the docking model with the Coq5-SAM structure allowed us to identify Arg201 and a water molecule (Wat1) near the C5 atom of the analogue, thus leading us to propose a catalytic mechanism for Coq5. In addition, we identified a putative $DDMQH_2$ substrate-entrance tunnel using *CAVER* (Chovancova *et al.*, 2012). After a remodelling process, we obtained an output cluster containing seven members, among which we chose the one with the lowest energy. In this model, a dumbbell-shaped tunnel from the protein surface to the active site was guarded by two α-helices (α1 and α7; Fig. 5*b*).

[1] Supporting information has been deposited in the IUCr electronic archive (Reference: KW5090).

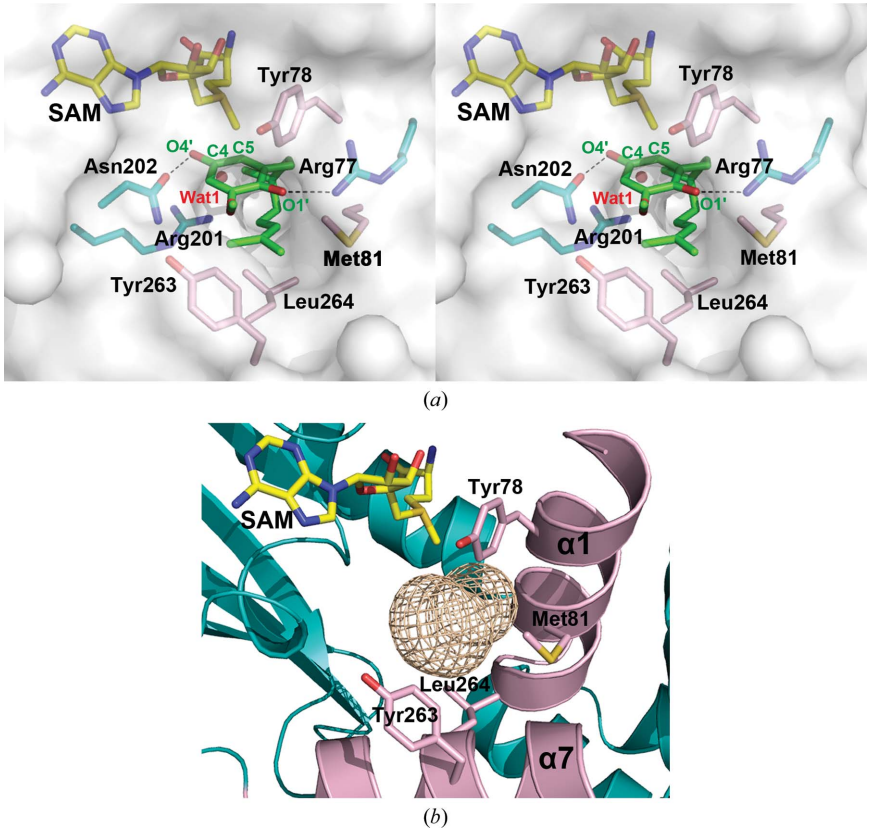

Figure 5
Simulation of the $DDMQH_2$ substrate-analogue binding model. (*a*) Stereoview of the simulated model of the $DDMQH_2$ substrate analogue in the binding cavity. (*b*) A putative substrate-entrance tunnel calculated by *CAVER* is denoted as a wheat mesh. Two α-helices (α1 and α7) are shown in pink and residues Tyr78, Met81, Tyr263 and Leu264 are shown as pink sticks. The protein is shown in the same orientation in all figures.

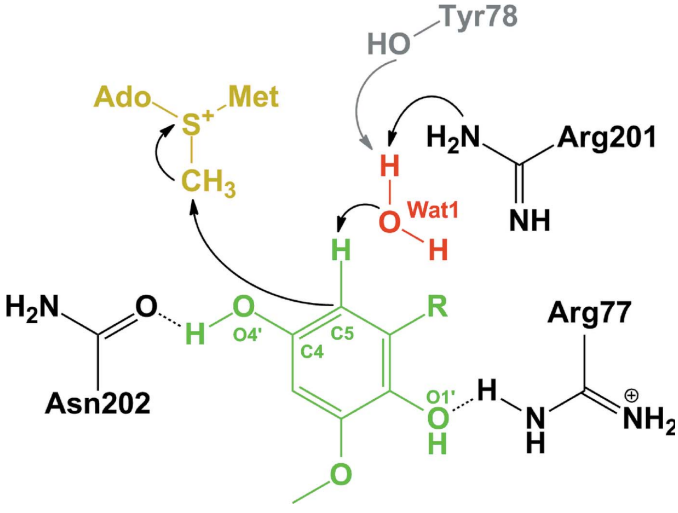

Figure 6
Putative catalytic mechanism of Coq5. SAM is shown in gold. The $DDMQH_2$ substrate is shown in green and *R* represents the polyprenyl side chain. Wat1 is shown in red and the side chains of Arg77, Arg201 and Asn202 are shown in black. In addition, Tyr78 is shown in grey, representing another possible catalytic base. Hydrogen bonds are illustrated as black dashed lines. Putative electron transfers are indicated by curved arrows.

From a closer viewpoint, we found that the three hydrophobic residues Tyr78, Met81 and Leu264 are located in the gorge of this tunnel. Additionally, another aromatic residue Tyr263 located at the solvent-exposed gate of the tunnel is also very likely to contribute to the hydrophobic environment. All of the residues forming the $DDMQH_2$ substrate-analogue binding pocket are highly conserved (Fig. 3).

3.4. A putative catalytic mechanism for Coq5

Based on these structural analyses, we proposed a catalytic mechanism for Coq5 (Fig. 6). Initially, Arg201 acts as a general base to abstract a proton from a water molecule (Wat1). A negatively charged O atom is then formed to interact with the H atom on the C5 atom of the $DDMQH_2$ substrate, thus initiating deprotonation of the C5 atom prior to methyl transfer. Hence, Arg201 is most likely to be a crucial residue to drive the water molecule Wat1 for catalysis. Moreover, the hydrogen bond between the hydroxyl group on the C4 atom of the $DDMQH_2$ substrate and the side chain of Asn202 may trigger the formation of the O4′ anion, which could in turn enhance the stability of the C5 anion by delocalizing the negative charge through an expanded network of conjugated π bonds. Alternatively, Tyr78 may be the catalytic base owing to the fact that many other methyltransferases adopt tyrosine as the general base (Huang *et al.*, 2002; Takata *et al.*, 2003; Lee *et al.*, 2012). Indeed, Tyr78, Arg201 and Asn202 are invariant in Coq5 homologues (Fig. 3). However, further site-directed mutagenesis and biochemical analyses are still required for validation of this hypothetical catalytic mechanism, given the availability of a proper substrate or analogue.

We thank the beamline staff of the Shanghai Synchrotron Radiation Facility (SSRF) for technical help during X-ray data collection. This work was supported by Project 2012CB911000 from the Ministry of Science and Technology of China, grant 31170695 from the National Natural Science Foundation of China and the Program for Changjiang Scholars and Innovative Research Team in University.

References

Adams, P. D. *et al.* (2010). *Acta Cryst.* D**66**, 213–221.
Baba, S. W., Belogrudov, G. I., Lee, J. C., Lee, P. T., Strahan, J., Shepherd, J. N. & Clarke, C. F. (2004). *J. Biol. Chem.* **279**, 10052–10059.
Battye, T. G. G., Kontogiannis, L., Johnson, O., Powell, H. R. & Leslie, A. G. W. (2011). *Acta Cryst.* D**67**, 271–281.

Binz, T. M., Maffioli, S. I., Sosio, M., Donadio, S. & Müller, R. (2010). *J. Biol. Chem.* **285**, 32710–32719.
Braun, S. D., Hofmann, J., Wensing, A., Ullrich, M. S., Weingart, H., Völksch, B. & Spiteller, D. (2010). *Appl. Environ. Microbiol.* **76**, 2500–2508.
Brindley, A. A., Raux, E., Leech, H. K., Schubert, H. L. & Warren, M. J. (2003). *J. Biol. Chem.* **278**, 22388–22395.
Carney, A. E. & Holden, H. M. (2011). *Biochemistry*, **50**, 780–787.
Chen, H., Zhao, Z., Hallis, T. M., Guo, Z. & Liu, H. (2001). *Angew. Chem. Int. Ed.* **40**, 607–610.
Chovancova, E., Pavelka, A., Benes, P., Strnad, O., Brezovsky, J., Kozlikova, B., Gora, A., Sustr, V., Klvana, M., Medek, P., Biedermannova, L., Sochor, J. & Damborsky, J. (2012). *PLoS Comput. Biol.* **8**, e1002708.
Crnovcić, I., Süssmuth, R. & Keller, U. (2010). *Biochemistry*, **49**, 9698–9705.
Chen, V. B., Arendall, W. B., Headd, J. J., Keedy, D. A., Immormino, R. M., Kapral, G. J., Murray, L. W., Richardson, J. S. & Richardson, D. C. (2010). *Acta Cryst.* D**66**, 12–21.
Emsley, P. & Cowtan, K. (2004). *Acta Cryst.* D**60**, 2126–2132.
Engh, R. A. & Huber, R. (1991). *Acta Cryst.* A**47**, 392–400.
Fawaz, F. & Jones, G. H. (1988). *J. Biol. Chem.* **263**, 4602–4606.
Fu, Z., Hu, Y., Konishi, K., Takata, Y., Ogawa, H., Gomi, T., Fujioka, M. & Takusagawa, F. (1996). *Biochemistry*, **35**, 11985–11993.
Grove, T. L., Benner, J. S., Radle, M. I., Ahlum, J. H., Landgraf, B. J., Krebs, C. & Booker, S. J. (2011). *Science*, **332**, 604–607.
Hao, Q., Gu, Y. X., Zheng, C. D. & Fan, H. F. (2000). *J. Appl. Cryst.* **33**, 980–981.
Hegazi, M. F., Borchardt, R. T. & Schowen, R. L. (1979). *J. Am. Chem. Soc.* **101**, 4359–4365.
Hsieh, E. J., Gin, P., Gulmezian, M., Tran, U. C., Saiki, R., Marbois, B. N. & Clarke, C. F. (2007). *Arch. Biochem. Biophys.* **463**, 19–26.
Huang, C. C., Smith, C. V., Glickman, M. S., Jacobs, W. R. & Sacchettini, J. C. (2002). *J. Biol. Chem.* **277**, 11559–11569.
Johnstone, L. A., Morgan, R. K., Marbois, B. N., Clarke, C. F. & Shepherd, J. N. (2007). *Abstr. Pap. Am. Chem. Soc.* **233**, 357.
Krissinel, E. & Henrick, K. (2007). *J. Mol. Biol.* **372**, 774–797.
Laskowski, R. A., MacArthur, M. W., Moss, D. S. & Thornton, J. M. (1993). *J. Appl. Cryst.* **26**, 283–291.
Lee, J.-H., Bae, B., Kuemin, M., Circello, B. T., Metcalf, W. W., Nair, S. K. & van der Donk, W. A. (2010). *Proc. Natl Acad. Sci. USA*, **107**, 17557–17562.
Lee, P. T., Hsu, A. Y., Ha, H. T. & Clarke, C. F. (1997). *J. Bacteriol.* **179**, 1748–1754.
Lee, S. G., Kim, Y., Alpert, T. D., Nagata, A. & Jez, J. M. (2012). *J. Biol. Chem.* **287**, 1426–1434.
Mahlert, C., Kopp, F., Thirlway, J., Micklefield, J. & Marahiel, M. A. (2007). *J. Am. Chem. Soc.* **129**, 12011–12018.
Martin, J. L. & McMillan, F. M. (2002). *Curr. Opin. Struct. Biol.* **12**, 783–793.
Morris, G. M., Huey, R., Lindstrom, W., Sanner, M. F., Belew, R. K., Goodsell, D. S. & Olson, A. J. (2009). *J. Comput. Chem.* **30**, 2785–2791.
Murshudov, G. N., Skubák, P., Lebedev, A. A., Pannu, N. S., Steiner, R. A., Nicholls, R. A., Winn, M. D., Long, F. & Vagin, A. A. (2011). *Acta Cryst.* D**67**, 355–367.
Pierrel, F., Hamelin, O., Douki, T., Kieffer-Jaquinod, S., Mühlenhoff, U., Ozeir, M., Lill, R. & Fontecave, M. (2010). *Chem. Biol.* **17**, 449–459.
Schubert, H. L., Blumenthal, R. M. & Cheng, X. (2003). *Trends Biochem. Sci.* **28**, 329–335.
Schüttelkopf, A. W. & van Aalten, D. M. F. (2004). *Acta Cryst.* D**60**, 1355–1363.
Takata, Y., Huang, Y., Komoto, J., Yamada, T., Konishi, K., Ogawa, H., Gomi, T., Fujioka, M. & Takusagawa, F. (2003). *Biochemistry*, **42**, 10874.
Tauche, A., Krause-Buchholz, U. & Rödel, G. (2008). *FEMS Yeast Res.* **8**, 1263–1275.
Tran, U. C. & Clarke, C. F. (2007). *Mitochondrion*, **7**, S62–S71.
Vagin, A. & Teplyakov, A. (2010). *Acta Cryst.* D**66**, 22–25.
Vidgren, J., Svensson, L. A. & Liljas, A. (1994). *Nature (London)*, **368**, 354–358.
Winn, M. D. *et al.* (2011). *Acta Cryst.* D**67**, 235–242.
Woodard, R. W., Mascaro, L., Hoerhammer, R., Eisenstein, S. & Floss, H. G. (1980). *J. Am. Chem. Soc.* **102**, 6314–6318.
Woodard, R. W., Tsai, M.-D., Floss, H. G., Crooks, P. A. & Coward, J. K. (1980). *J. Biol. Chem.* **255**, 9124–9127.
Wu, J. C. & Santi, D. V. (1987). *J. Biol. Chem.* **262**, 4778–4786.